Solving Kinetic Equations for the Laser Flash Photolysis Experiment on Nitric Oxide Synthases: Effect of Conformational Dynamics on the Interdomain Electron Transfer

**Andrei V. Astashkin**[†] and **Changjian Feng**[‖,*]

[†]Department of Chemistry and Biochemistry, University of Arizona, Tucson, AZ 85721, USA

[‖]College of Pharmacy, University of New Mexico, Albuquerque, NM 87131, USA

Abstract

The production of nitric oxide by the nitric oxide synthase (NOS) enzyme depends on the interdomain electron transfer (IET) between the flavin mononucleotide (FMN) and heme domains. Although the rate of this IET has been measured by laser flash photolysis (LFP) for various NOS proteins, no rigorous analysis of the relevant kinetic equations was performed so far. In this work, we provide an analytical solution of the kinetic equations underlying the LFP approach. The derived expressions reveal that the bulk IET rate is significantly affected by the conformational dynamics that determines the formation and dissociation rates of the docking complex between the FMN and heme domains. We show that in order to informatively study the electron transfer across the NOS enzyme, LFP should be used in combination with other spectroscopic methods that could directly probe the conformational rate constants. The implications of the obtained analytical expressions for the interpretation of the LFP results from various native and modified NOS proteins are discussed. The mathematical formulae derived in this work should also be applicable for interpreting the IET kinetics in other modular redox enzymes.

Abstract
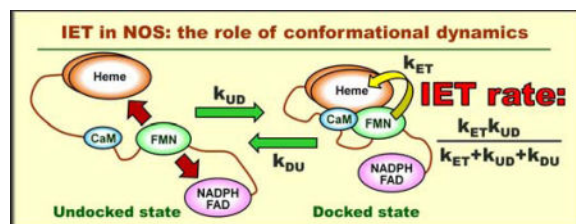
Introduction

Mammalian nitric oxide synthase (NOS) enzyme catalyzes the 5-electron oxidation of L-arginine (L-Arg) to NO and citrulline, utilizing NADPH and O_2 as co-substrates.[1–2]

CORRESPONDING AUTHOR: Changjian Feng, cfeng@unm.edu; phone: 505-925-4326; fax: 505-925-4549.

Structurally, NOS is a homodimeric protein, each monomer of which consists of a C-terminal electron-supplying reductase domain and an N-terminal catalytic heme-containing oxygenase domain (the terms 'oxygenase domain' and 'heme domain' are interchangeable). The reductase domain consists of a ferredoxin-NADP reductase (FNR) (sub)domain, which contains binding sites for NADPH (the electron source) and flavin adenine dinucleotide (FAD), and a flavin mononucleotide (FMN) (sub)domain. The FMN domain is connected to the FNR and heme domains by flexible linkers, which allow it to shuttle between these terminal domains to deliver the NADPH-derived electrons to the heme active site[3] where the NO production takes place.[4]

The interdomain electron transfer (IET) processes represent key steps in NOS catalysis.[1, 5–6] They are regulated by calmodulin (CaM), which binds to the CaM-binding region of the linker joining the FMN and heme domains. Although the CaM binding to NOS has little to no effect on the thermodynamics of redox processes,[7–9] it facilitates the IET from the FAD hydroquinone to FMN semiquinone (FMNH$^\bullet$) within the reductase domain[10] and enables the IET from the FMN hydroquinone (FMN$_{hq}$) to the catalytic heme iron in the heme domain.[3] This indicates that the NOS regulation by CaM is accomplished dynamically through controlling conformational changes required for effective IET.[11–13]

As a direct way to measure the bulk FMN–heme IET rate in NOS, a laser flash photolysis (LFP) approach was applied to wild type (wt) and mutant NOS enzymes of different isoforms and domain composition (constructs).[14–22] So far, rigorous analysis of the LFP data using the relevant kinetic equations has not been carried out. In particular, it was not mathematically clear, how the contributions of the intrinsic IET rate constants and those describing the conformational dynamics determine the observed (bulk) IET rate. In this work, we put the analysis of LFP experimental results on a solid mathematical ground by providing an analytical solution of the kinetic equations in terms of the IET rate constants and presenting approximate practical expressions that reveal the important relationship between the bulk IET rate and the conformational dynamics in NOS. In comparison with an earlier broadly related work on the IET in tethered proteins by Kawatsu and Beratan,[23] our treatment is focused on the NOS system and the LFP approach and includes the reversible IET and the gradual return of the system to the pre-IET state. The use of the obtained expressions for the interpretation of the LFP results is discussed.

Results and discussion

1. Structural interconversions in NOS

The IET process in the CaM-bound full-length NOS is a composite result of the enzyme cycling through several conformational states (see Figure 1):[6, 24]

i.   The input state, where the FMN domain is docked to the FNR domain containing the binding sites for FAD and NADPH. In this state, the NADPH-derived electron is transferred into FMN through FAD.

ii.   The intermediate (free) state, where the FMN domain is undocked from both the FNR and heme domains. This is the state of a large-scale motion between the

two docking positions and is characterized by a broad dynamic conformational distribution.

iii. The output state, where the FMN domain is docked to the heme domain. This is the state where the FMN – heme IET takes place and the electron is transferred out of the FMN domain.

Since the FMN–heme IET event takes place in the FMN – heme docked state (the output state in Figure 1), for the purposes of this work, we can single this state out and refer to it simply as the docked state (denoted by D, see Figure 1). The input and intermediate states will be combined into a single undocked (with respect to the FMN-heme domain docking) state and denoted by U.

2. IET kinetics in a laser flash photolysis experiment

We will specifically formulate the FMN–heme IET kinetics problem in the context of the LFP experiment. In this experiment, NOS is initially in the IET-inactive [Fe(III)][FMN] state (I in Figure 2). The IET-ready state, R, is prepared by an appropriate period (seconds) of illumination of the sample with white light. At the R state, the heme center is ferrous, with the CO ligand bound to the Fe(II) ion, while the FMN center is partially reduced to FMN semiquinone, $FMNH^{\bullet}$. The IET is not possible, however, because of the presence of CO ligand at the heme center. The IET-active state, A, is achieved by a short (2–3 ns) laser pulse at 446 nm, which releases the CO ligand from the heme center. The laser-induced CO dissociation results in a drop of the midpoint potential of the heme and converts a good electron acceptor (the Fe(II)–CO complex) into an electron donor (the CO-free Fe(II) species) favoring the electron transfer (ET) from Fe(II) to $FMNH^{\bullet}$. As a result of the heme-FMN IET, the active state is converted to the final [Fe(III)][FMN_{hq}] state, F. A competing process of CO rebinding also converts the active state back to the ready state. Thus, the I, R, A, and F states differ mainly in the redox states of the heme iron and FMN centers, although the difference between A and R is in the CO-binding state of the ferrous heme center.

In Figure 2, U and D represent the FMN-heme undocked and docked states, respectively; k_{DU} and k_{UD} are, respectively, the D $\rightarrow$ U and U $\rightarrow$ D conformational interconversion constants; k_{ETf} and k_{ETb} are, respectively, the forward and backward intrinsic ET rates. In addition, the sum of k_{ETf} and k_{ETb} will be denoted as k_{ET}. The A $\rightarrow$ R conversion caused by the CO rebinding to the heme is shown by a dashed arrow. The corresponding rate constant is denoted by k_{AR}. In addition to the formal kinetic description, the following important physical details about the conformational and intrinsic ET rate constants and the docked state should be noted:

i. k_{UD} represents the diffusion-controlled frequency of productive collisions between the FMN and heme domains, where "productive" means the collisions that lead to the formation of the docked state. As such, it depends on viscosity, the presence or absence of the FNR domain in the studied NOS protein (full-length enzyme *vs.* bi-domain oxygenase-FMN construct, *i.e.*, the oxyFMN construct), CaM-dependent conformational flexibility limitations, as well as other factors, including the ionic interactions between the charged surface residues of the FMN and heme domains.

ii. k_{DU} represents the inverse lifetime of the docking complex. This lifetime is mostly determined by the FMN-heme domain specific interactions, but it can also be affected by the presence or absence of the FNR domain in the studied NOS enzyme. In addition, the docking interaction between CaM and the heme domain facilitates the formation of the FMN - heme domain docking complex[25] and is expected to decrease k_{DU}.

iii.   Most likely, the docking conformation itself exhibits a certain structural disorder (extremely minor compared to the broad structural distribution of the undocked state), with constant interconversions between the docked sub-states[23]. The position changes in this process of "conformational sampling" are relatively small and may not be clearly distinguishable in an experiment (*i.e.*, the experiment will only detect that the domains are in close contact, with the interdomain distance and relative orientation being distributed in narrow limits of just a few Å and degrees). The efficient interdomain electron tunneling only happens within a narrow range of possible docking conformations, and thus the time spent on conformational sampling contributes to the intrinsic IET rate constants, k_{ETf} and k_{ETb}, and can make them orders of magnitude smaller than the ideal IET rate constants estimated using the protein ET theory (see, *e.g.*, ref.[26–27]).

iv.   Like any diffusion process, the conformational sampling in the docked state is mass-dependent. The FNR domain represents an additional mass connected to the FMN domain by a linker, and therefore, it may hinder the conformational sampling and result in slower intrinsic IET rates in a full-length NOS as compared with the bi-domain oxyFMN construct. Because of the linker, the effect should be smaller than for a rigid connection, but it cannot be excluded entirely.

The IET in the LFP experiment is monitored by following the change in the optical absorption at specific wavelengths where Fe(II) or FMNH$^{\bullet}$ dominates the spectrum.[6] In nNOS and iNOS, the Fe(II) oxidation was observed at 460 and 465 nm, respectively.[19–20] The consumption of FMNH$^{\bullet}$ was monitored at 580 – 600 nm.[21, 28] As both the ready and active states contain the FMN and heme species, the total absorbance at the selected wavelength λ, A_λ, can in general be expressed as:

$$A_\lambda = \varepsilon_A \cdot [A] + \varepsilon_R \cdot [R] \quad (1)$$

where ε_A and ε_R are the molar extinction coefficients in the active and ready states, respectively.

A typical $A_\lambda(t)$ trace detected in an LFP experiment is shown in Figure 3. During the initial stage (the IET phase) of the processes, [R] is close to zero and practically does not change, and the observed absorbance decrease is solely due to the depopulation of the active state caused by the A $\rightarrow$ F forward ET. As [A] decreases and [F] increases, the F $\rightarrow$ A backward ET starts competing with the forward ET, which eventually leads to an equilibration of the

active and final state populations. The observed absorbance change in the IET phase is usually monoexponential, and the bulk IET rate constant is denoted k_{IET}. The total absorbance change in this process is referred to as the IET amplitude.

At a longer time scale, the slow CO rebinding process starts gradually converting the A state back to the R state. The decreasing A state population is replenished from the F state "while supplies last". At the end, the system completely converts back to the ready state. This increase of [R] is evidenced by the increase of A_λ to the pre-IET state (see Figure 3). The rate constant describing the CO rebinding process determined from this part of the kinetics is denoted k_{CO}. The main goal of this work is to establish the relationship between the observed rate constants (k_{IET} and k_{CO}) and the intrinsic rate constants indicated in Figure 2.

When the IET is initiated by a laser pulse, the system is in a conformational equilibrium, with populations of the docked and undocked states being:

$$[D]_o = k_{UD}[NOS]/(k_{UD}+k_{DU}); \qquad [U]_o = k_{DU}[NOS]/(k_{UD}+k_{DU}) \quad (2)$$

where [NOS] is the total NOS concentration. The initial populations of the ready and final states are $[R]_o = 0$ (the system in the laser excited region is fully converted to the active state by the laser pulse) and $[F]_o = 0$. These initial populations, along with all necessary starting time derivatives that are readily calculated from the kinetic equations (see below), are used to calculate the pre-exponential factors in the solutions of the kinetic equations.

The kinetic equations describing the processes indicated by arrows in Figure 2 are:

$$[\dot{U}] = -(k_{UD}+k_{AR})[U]+k_{DU}[D]$$

$$[\dot{D}] = k_{UD}[U] - (k_{DU}+k_{ETf}+k_{AR})[D]+k_{ETb}[D_F]$$

$$[\dot{D}_F] = k_{ETf}[D] - (k_{ETb}+k_{DU})[D_F]+k_{UD}[U_F] \quad (3)$$

$$[\dot{U}_F] = -k_{UD}[U_F]+k_{DU}[D_F]$$

$$[\dot{R}] = k_{AR}([U]+[D])$$

In these equations, the docked and undocked conformations in the final state are denoted by D_F and U_F, respectively, to distinguish them from the corresponding conformations in the active state (see Figure 2). Note that the CO rebinding is described as pseudo-first-order, although actually it is a bimolecular process with the rate determined by $k_{bm}[NOS][CO]$,

where k_{bm} is a bimolecular rate constant. This simplification is valid because the CO concentration (mM level) is much larger than that of NOS (10–20 μM), and thus k_{AR} in Eqs. 3 represents the product: $k_{AR} = k_{bm}[CO]$.

Given the large number of kinetic equations, the simplicity of the experimental LFP trace (Figure 3) appears striking. For example, the IET phase of the kinetics is expected to be described by up to four exponential functions, but only one is generally observed. As shown below, the reason for this simplicity is the fact that only one exponential function is slow enough to be resolved and/or has large enough amplitude to be reliably detected against the noise level. In this situation, the LFP experiment can only yield a certain combination of the intrinsic rate constants, which corresponds to the observed bulk IET rate. As a result, although the experimental LFP traces can be simulated by solving Eqs. 3 numerically, the kinetic parameters obtained will not be unique. The analytical solution of Eqs. 3 will provide a practical expression that can be used for good initial estimates of the intrinsic rate constants, including the range of their variation, which would potentially fit the experimental LFP kinetics. It will also help better understand the kinetic information obtainable in a typical LFP experiment.

The analytical solution of the full set of the equations involves finding roots of the fourth order polynomial (actually a fifth order polynomial, one of the roots of which is zero). While this is possible (*e.g.*, through a combination of resolvent cubic and Cardano methods), such a solution will not be useful for simple practical estimates because of its bulkiness and either the use of trigonometric functions or multiple cubic and square roots. We will therefore provide an approximate solution employing the fact that in practice the CO rebinding rate is usually much slower than the IET rate (see, *e.g.*, Figure 3). We will approach the problem in two stages, first considering the interconversion between the A and F states without the CO rebinding ($k_{AR} = 0$), and then accounting for the slow CO rebinding, while maintaining an approximate equilibrium between the U and D conformations within the active and final states.

3. IET without CO rebinding: $k_{AR} = 0$

We will first consider the kinetics without the CO rebinding. Solving Eqs. 3 with $k_{AR} = 0$ gives three non-zero rate constants:

$$k_c = k_{UD} + k_{DU}; \qquad k_+ = \frac{k_s}{2} + \sqrt{\frac{k_s^2}{4} - k_p} \qquad k_- = \frac{k_s}{2} - \sqrt{\frac{k_s^2}{4} - k_p} \qquad (4)$$

where $k_s = k_{UD} + k_{DU} + k_{ET}$, $k_p = k_{ET} k_{UD}$, and $k_{ET} = k_{ETf} + k_{ETb}$. The subscripts "s" and "p" in k_s and k_p stand for "sum" and "product", respectively. The subscript "c" in k_c stands for "conformational" and refers to the fact that k_c is the rate constant responsible for establishing the U $\leftrightarrow$ D conformational equilibrium.

The active and final state populations are:

$$[A] = A_+ \exp(-k_+ t) + A_- \exp(-k_- t) + A_\infty; \quad [F] = [NOS] - [A] \quad (5)$$

where:

$$A_+ = \frac{k_{ETf}}{k_+ - k_-} \cdot \left(\frac{k_{UD}}{k_c} - \frac{k_-}{k_{ET}} \right) \cdot [NOS];$$

$$A_- = \frac{k_{ETf}}{k_+ - k_-} \cdot \left(\frac{k_+}{k_{ET}} - \frac{k_{UD}}{k_c} \right) \cdot [NOS]; \quad (6)$$

$$A_\infty = \frac{k_{ETb}}{k_{ET}} \cdot [NOS]$$

There is no exponent with k_c in Eq. 5 (*i.e.*, its amplitude equals zero) because this rate constant is responsible for maintaining the U $\leftrightarrow$ D conformational equilibrium, which exists at the start and is conserved in the IET reactions: [U] + [U_F] and [D] + [D_F] are expressed only through each other using the k_{UD} and k_{DU} conformational rate constants.

Let us consider the rates and amplitudes of the contributing exponential functions in more detail. One can readily estimate:

$$\frac{k_s^2}{k_p} = \frac{k_{UD}}{k_{ET}} + \frac{k_{DU}^2}{k_{UD} k_{ET}} + \frac{k_{ET}}{k_{UD}} + 2 + 2\frac{k_{DU}}{k_{ET}} + 2\frac{k_{DU}}{k_{UD}} = = 2(1 + r_{UD}) + \left((1 + r_{UD})^2 \frac{k_{UD}}{k_{ET}} + \frac{k_{ET}}{k_{UD}} \right) \geq 4(1 + r_{UD})$$

$$(7)$$

where $r_{UD} = [U]_o/[D]_o = k_{DU}/k_{UD}$. The final inequality in Eq. 7 is obtained by considering the sum in parentheses, which attains its minimum at $k_{ET}/k_{UD} = 1 + r_{UD}$. The pulsed EPR[29] and fluorescence lifetime[30–33] measurements show that in the CaM-bound NOS, r_{UD} 2 (*i.e.*, [D]$_o$ ~ 35% or less, depending on the NOS isoform, mutation, and presence or absence of the FNR domain; see Table 1), which immediately results in $k_s^2/k_p \geq 12$. The square root in Eq. 4 can therefore be expanded with the accuracy to the terms linear in k_p/k_s^2 to give:

$$k_+ = k_s - \frac{k_p}{k_s} \approx k_s; \qquad k_- = \frac{k_p}{k_s} \quad (8)$$

which shows that $k_+ \gg k_- (k_+/k_- \approx k_s^2/k_p \geq 12)$.

The exponential term corresponding to k_+ describes the fast IET from (mostly) the docked state existing at the time of the laser pulse. This term has a small amplitude: since $k_+ \gg k_-$ and $k_{UD} < (\ll) k_{DU}$, it follows that for the general case, $k_{ETf}/(k_+ - k_-) \approx 1$, and $k_{UD}/k_c \approx k_{UD}/k_{DU} > k_-/k_{ET} \sim k_{UD}/(k_c+k_{ET})$, which results in $A_+ \sim (k_{UD}/k_{DU}) \cdot [\text{NOS}] < (\ll) A_-$. The k_+ term may also be exceedingly fast to be detectable in a routine LFP experiment.

The largest pre-exponent corresponds to the k_- term, which describes the IET from (mostly) the state A population that is in the undocked conformation at the time of the laser pulse. Obviously, to engage in the ET process, these molecules should first achieve the docked conformation. The active state population kinetics is thus approximately monoexponential, and k_- corresponds to the effective IET rate constant, k_{IET}, obtained in LFP measurements (see Figure 3). Equating k_{IET} with k_- one can write:

$$[A] \approx [\text{NOS}] \cdot \left(\frac{k_{ETb}}{k_{ET}} + \frac{k_{ETf}}{k_{ET}} \exp(-k_{IET}\, t) \right) \quad (9)$$

where $k_{IET} = k_-$:

$$k_{IET} = \frac{k_s}{2} - \sqrt{\frac{k_s^2}{4} - k_p} \approx \frac{k_{ET}\, k_{UD}}{k_{ET} + k_{UD} + k_{DU}} \quad (10)$$

Equation 10 represents a compilation of the expressions for k_- in Eqs. 4 and 8 and is given for convenience of future reference.

As an example, Figure 4 shows the calculated active state population for $k_{DU} = 10\ \text{ms}^{-1}$, $k_{UD} = 3.33\ \text{ms}^{-1}$ ($r_{UD} = 3$), and three different intrinsic IET rates corresponding to $k_{ET} \gg k_{DU}$, $k_{ET} = k_{DU}$, and $k_{ET} \ll k_{DU}$ (panels a, b, and c, respectively). To maximize the change in [A], the calculations were performed for $k_{ETb} = 0$. Assuming $k_{ETb} > 0$ while keeping k_{ET} the same would only result in a decreased amplitude of the overall time-dependent part of [A](t) because k_+, k_-, and A_+/A_- only depend on k_{ET} (see Eqs. 4 and 5).

The black trace in each panel of Figure 4 represents an exact solution of Eqs. 3 calculated using Eqs. 5 and 6. The green trace represents a monoexponential approximation given by Eq. 9, with k_{IET} calculated using the exact expression in Eq. 10. The red trace again represents a monoexponential approximation given by Eq. 9, but with k_{IET} calculated using the approximate expression in Eq. 10. Thus, the comparison between the black and green traces shows the accuracy of a monoexponential approximation. The comparison between the green and red traces tests the accuracy of the approximate formula for k_{IET} in Eq. 10.

One can see that after the initial fast decay (with the relative amplitude of $\sim k_{UD}/k_{DU}$ in panel a and progressively smaller in panels b and c), the monoexponential model provides a good description of the IET kinetic. The exact and approximate k_{IET} values obtained from Eq. 10 are very close to each other. The largest difference between them is observed for Figure 4b, and it only amounts to about 7%.

The calculations shown in Figure 4 were performed for $r_{UD} = 3$. The increase in r_{UD} improves both the monoexponential character of the overall kinetics and the agreement between the exact and approximate estimates of k_{IET}. The decrease in r_{UD} obviously has the opposite effect, but even for $r_{UD} = 1$ the largest difference between the exact and approximate k_{IET} estimates is only 15%, and although the contribution of the fast exponent to the exact kinetics calculated using Eq. 5 increases (~40% for $k_{ET} \gg k_{UD}$), the trace is still monoexponential for over 90% of the observable timebase. The examples of the calculations for $r_{UD} = 10$ and $r_{UD} = 1$ are given in Supporting Information.

4. Accounting for the CO rebinding: $k_{AR} \neq 0$

In the presence of CO rebinding, the analytical solution of the full kinetic problem becomes problematic even in terms of obtaining the approximate expressions. The situation is dramatically simplified, however, by the fact that the rate of CO rebinding process is usually much slower than the observed IET rate (see, *e.g.*, Figure 3).[14–22] Since $k_{IET} \approx k_{UD} < (\ll) k_{UD}+k_{DU}$ (see Eq. 10), the A and F states during the CO rebinding process approximately maintain their U $\leftrightarrow$ D conformational equilibria. One can thus formulate the problem in terms of the interconversions between the active, ready, and final states, without breaking them down into the docked and undocked conformations:

$$[\dot{R}] = k_{AR}[A]$$

$$[\dot{A}] = -(k_{AR}+k_{AF})[A]+k_{FA}[F] \quad (11)$$

$$[\dot{F}] = k_{AF}[A] - k_{FA}[F]$$

where k_{AF} and k_{FA} are the rate constants for the A $\rightarrow$ F and F $\rightarrow$ A transitions (accomplished by IET), respectively. Since the A and F states are close to their internal conformational equilibria, these rate constants are obviously equal to:

$$k_{AF} = \frac{k_{UD}}{k_{UD}+k_{DU}} \cdot k_{ETf}; \qquad k_{FA} = \frac{k_{UD}}{k_{UD}+k_{DU}} \cdot k_{ETb} \quad (12)$$

(as obtained from, *e.g.*, $k_{AF}[A] = k_{ETf}[D]$). The solution of Eqs. 11 gives two non-zero rate constants:

$$k_{CO+} = \frac{k_{COs}}{2} + \sqrt{\frac{k_{COs}^2}{4} - k_{COp}} \qquad k_{CO-} = \frac{k_{COs}}{2} - \sqrt{\frac{k_{COs}^2}{4} - k_{COp}} \quad (13)$$

where $k_{COs} = k_{AF} + k_{FA} + k_{AR}$ and $k_{COp} = k_{AR}k_{FA}$ ("s" and "p" in the subscripts stand for "sum" and "product"). Since $k_{AR} \ll (k_{AF}, k_{FA})$, and thus $(k_{COs})_2 \gg k_{COp}$, one obtains:

$$k_{CO+} \approx k_{COs} = k_{AR} + \frac{k_{ET}}{1 + r_{UD}}; \qquad\qquad k_{CO-} \approx \frac{k_{COp}}{k_{COs}} = \frac{k_{AR} k_{ETb}}{k_{AR}(1 + r_{UD}) + k_{ET}} \qquad (14)$$

The larger rate constant, k_{CO+}, is responsible for maintaining the equilibrium between the A and F states, which the slow A → R process described by k_{CO-} tries to disbalance. The amplitude of the exponent corresponding to k_{CO+} in the solutions for [A], [R], and [F] is proportional to k_{AR}/k_{ET} ($\lll$ 1).

The larger pre-exponent corresponds to the k_{CO-} term, which describes the slow repopulation of the R state and the corresponding depopulation of the A and F states due to the CO rebinding process. The CO rebinding kinetics is thus approximately monoexponential, and k_{CO-} corresponds to the apparent CO rebinding rate constant, k_{CO}, obtained in the LFP measurements (see Figure 3). Equating k_{CO} with k_{CO-}, one can write:

$$[R] \approx [NOS] \cdot (1 - \exp(-k_{CO} t)); \qquad\qquad [A] \approx [NOS] \cdot \frac{k_{ETb}}{k_{ET}} \cdot \exp(-k_{CO} t); \qquad (15)$$

and [F] = [NOS] − [A] − [R]. In these expressions, $k_{CO} = k_{CO-}$:

$$k_{CO} = \frac{k_{COs}}{2} - \sqrt{\frac{k_{COs}^2}{4} - k_{COp}} \approx \frac{k_{AR} k_{ETb}}{k_{AR}(1 + r_{UD}) + k_{ET}} \qquad (16)$$

Equation 16 represents a compilation of the expressions for k_{CO-} in Eqs. 13 and 14 and is given for convenience of future reference.

It follows from Eqs. 15 and 16 that the slow conversion of the NOS population to the ready state is only possible with $k_{ETb} > 0$. If $k_{ETb} = 0$, then also $k_{CO} = 0$, and [R] ≈ 0, as obtained from Eq. 15. In this case, however, Eq. 15 becomes insufficient, and one has to explicitly consider the rapid term described by k_{CO+}. Since for the rapid term the internal conformational equilibrium condition becomes invalid (because then $k_{CO+} = k_{COs} > k_{UD} + k_{DU}$), the problem has to be solved with the explicit account of the conformational interconversions in the active state (for $k_{ETb} = 0$, the internal conformational dynamics of the final state is not important). The rigorous analysis of the situation with $k_{ETb} = 0$ (see Supporting Information) shows that in this case the population transferred to the ready state is very small (~ k_{AR}/k_{IET}) because the slow CO rebinding competes with a much faster IET process. This small population transfer from the active to the ready state occurs with the characteristic rate constant $k_{AR} + k_{IET} \approx k_{IET}$ (where k_{IET} is given by Eq. 10), *i.e.*, with the same rate as the observed IET process. The slow component, k_{CO}, is obviously not observed in this case.

As an example, Figure 5 shows a comparison between the total population of A and R states obtained by a numerical solution of Eqs. 3 with the approximate [A]+[R] values estimated using Eqs. 15 (see Supporting Information for the numerical solution details). The

calculations correspond to $k_{DU} = 10$ ms^{-1}; $k_{UD} = 3$ ms^{-1}; $k_{ETf} = k_{ETb} = 5$ ms^{-1}; $k_{AR} = 0.03$, 0.3, and 1 ms^{-1} in panels a, b, and c, respectively. The black trace in each panel represents a numerical solution of Eqs. 3. The green trace represents a monoexponential approximation given by Eqs. 15, with k_{CO} calculated using the exact (for the internal equilibrium model) expression in Eq. 16. The red trace again represents a monoexponential approximation given by Eqs. 15, but with k_{CO} calculated using the approximate expression in Eq. 16. Thus, the comparison between the black and green traces shows the accuracy of the internal equilibrium model described by Eqs. 11. The comparison with the red trace tests the accuracy of the approximate formula for k_{CO} given by the second part of Eq. 16.

With increasing k_{AR}, as expected, the exact analytical solution using the equilibrium model becomes progressively further from the numerical solution of Eqs. 3: in panels a, b, and c, the slope of the green trace overestimates the asymptotic slope of the black trace by 0.4%, 4%, and 15%, respectively. As explained below, this overestimation of k_{CO} is mostly caused by the assumption of the internal conformational equilibrium in the F state. Interestingly, since the linear expansion of the square root in Eq. 16 underestimates the resulting rate constant, the approximate expression for k_{CO} is actually closer to the numerical solution than the exact one, the errors for panels a, b, and c being 0.3%, 1.4%, and 1.1%, respectively.

Since the active state converts back to the ready state with the rate constant k_{AR} from both conformations, U and D, the conformational equilibrium in the active state is not very important for the validity of the equilibrium model (*i.e.*, the first equation in Eqs. 11 is valid regardless of the internal equilibrium in the A state). On the other hand, the final state connects to the ready state through the ET from the docked conformation, D_F, to the active state. This one-ended connection makes maintaining the conformational equilibrium in the final state especially important for the validity of the equilibrium model. In practical terms, this means that the decrease in $[D_F]$ caused by the CO rebinding process should be timely compensated for by the net population transfer from the undocked state, U_F. Therefore, one can expect the equilibrium approximation to overestimate k_{CO} (by assuming instant conformational equilibration in the F state) and to become progressively poorer for k_{UD} comparable with or smaller than k_{AR}. Indeed, the calculation similar to that in Figure 5c, but with $k_{UD} = 1$ ms^{-1} results in the relative errors of the "exact" and "approximate" expressions of 45% and 24%, respectively. The condition $k_{UD} = k_{AR}$ thus represents an approximate applicability limit for the equilibrium model. In our discussion of the experimental data below we will show that this limit is practically never reached, and the equilibrium model in most cases is adequate for describing the CO rebinding process.

5. Using k_{IET} and k_{CO} for practical estimates

There are essentially three parameters that are measured in an LFP experiment: k_{IET} (Eq. 10), ΔA_λ, which is the change in A_λ due to the IET, and k_{CO} (Eq. 16). The intrinsic CO rebinding rate, k_{AR}, can be measured separately for the NOS heme domain (NOSoxy construct) using the same CO concentration as the actual IET measurements. One can compare this rate with k_{IET} to establish if the equilibrium approximation (Eqs. 11) is adequate for describing the CO rebinding process in the actual experiments. For all of the

NOS proteins listed in Table 1, with the exception of wt rat nNOS oxyFMN without CaM[21] and bovine eNOS,[17] k_{IET} is over 30 s^{-1}, while the measured k_{AR} values are about 10 s^{-1}.[21–22] Since $k_{IET} < k_{UD}$ (see Eq. 10), $k_{UD}/k_{AR} > 3$. For such k_{UD}/k_{AR} ratios, the approximate formula in Eq. 16 predicts the CO rebinding kinetics with the accuracy of ~ 1% or better (see, *e.g.*, the calculation in Figure 5c, which corresponds to $k_{UD}/k_{AR} = 3$), and thus the equilibrium model in the overwhelming majority of cases is appropriate for the description of the CO rebinding process. Should the validity of the equilibrium model for some sample become questionable, the LFP experiment can be repeated at a lower CO concentration. Since $k_{AR} \propto$ [CO], the decrease in [CO] can establish the conditions appropriate for the equilibrium model applicability.

Using the approximate expression in Eq. 16 and the experimental values of k_{AR} and k_{CO}, one can estimate the ratio of k_{ETb} and k_{ET} (and from there, k_{ETb}/k_{ETf}):

$$\frac{k_{ETb}}{k_{ET}} = \frac{k_{CO}}{k_{AR}} + \frac{k_{CO}(1+r_{UD})}{k_{ET}} \approx \frac{k_{CO}}{k_{AR}} \quad (17)$$

The relative accuracy of the approximate equality in Eq. 17 is obviously equal to $k_{AR}(1+r_{UD})/k_{ET}$. We will show below, when we discuss k_{IET}, that this approximation is sufficiently accurate for all practical purposes.

As an example, a comparison between k_{AR} and k_{CO} constants obtained in the same sets of experiments under identical conditions shows that k_{AR}/k_{CO} is close to 2 (10 s^{-1}/5.6 s^{-1} for NOSoxy/oxyFMN constructs of murine iNOS[22] or 10.6 s^{-1}/3.8 s^{-1} for rat nNOS[21]). It thus follows from Eq. 17 that $k_{ETb} \approx k_{ETf}$, which is in agreement with the expectations based on the fact that Fe(III)/Fe(II) and FMNH$^{\bullet}$/FMN$_{hq}$ are nearly isopotential.[34] One has to note, however, that caution should be exercised when correlating the intrinsic ET rates, k_{ETf} and k_{ETb}, with the redox potentials because these rates are also probably affected to a large degree by the conformational sampling (the adjustment of the domain alignment in the docking complex). Unfortunately, at this point, it is not possible to fully address this problem because the exact information about the absolute ET rates is not available (see below).

The "IET kinetic amplitude", A_{λ}, can also give information about the ratio of the forward and backward ET constants:

$$\Delta A_{\lambda} = \varepsilon_A([A]_o - [A]_{\infty}) = \varepsilon_A \cdot \frac{k_{ETf}}{k_{ET}} \cdot [NOS] = \frac{\varepsilon_A}{1 + k_{ETb}/k_{ETf}} \cdot [NOS] \quad (18)$$

where $[A]_o$ and $[A]\infty$ are the active state concentrations at $t = 0$ and $t \to \infty$ (or more practically, the time when [A] and [F] approximately equilibrate before the onset of the CO rebinding process), respectively. The accuracy of such estimates using A_{λ}, however, would be significantly lower because they require accurate knowledge of [NOS] and ε_A.

Let us now consider the observed IET rate constant, k_{IET}. If the intrinsic ET rate is much faster than the rates of conformational interconversions ($k_{ET} \gg k_{UD}, k_{DU}$) then Eq. 10 simplifies to $k_{IET} \approx k_{UD}$. In this case, the observed IET rate constant is obviously determined by the rate of formation of the docked state, k_{UD}. If k_{ET} is comparable with the docked state dissociation rate ($k_{ET} \sim k_{DU} > (\gg) k_{UD}$), then k_{IET} becomes sensitive to k_{DU}: $k_{IET} \approx k_{ET}k_{UD}/(k_{ET}+k_{DU})$. For still smaller k_{ET} ($k_{ET} \quad k_{UD} < (\ll) k_{DU}$), this trend continues, and the observed IET rate becomes highly sensitive to k_{DU}: $k_{IET} \approx k_{ET}k_{UD}/k_{DU}$. Similar approximate expressions were obtained for a bimolecular ET in the pseudo first order limit, when the acceptor concentration was considered much greater than that of the donor.[23]

To determine the intrinsic ET rate(s), one can rewrite the approximate equality in Eq. 11 as:

$$k_{ET} = \frac{k_{IET}(k_{UD}+k_{DU})}{k_{UD} - k_{IET}} \geq (1+r_{UD})k_{IET} \quad (19)$$

The conformational rate constants, k_{DU} and k_{UD}, are not known separately, and only their ratio, r_{UD}, has been measured (in the form of $[U]_o/[D]_o$ population ratio, see Eq. 2) for some of the NOS preparations by pulsed EPR and fluorescence lifetime measurements; see Table 1. Therefore, at this stage, one can only estimate the range of possible k_{ET} values corresponding to the value of k_{IET} measured in an experiment.

As follows from Eq. 10, $k_{IET} < k_{UD}$, but $k_{IET} \rightarrow k_{UD}$ for $k_{ET} \rightarrow \infty$. Conversely, assuming $k_{IET} = k_{UD}$ results in $k_{ET} = \infty$, which represents the upper limit of possible k_{ET} values. The lower limit is obtained by assuming $k_{IET} \ll k_{UD}$, in which case the minimal k_{ET} is given by the last expression in Eq. 19. To estimate the specific value of k_{ET}, an absolute measurement of the conformational rate constants is necessary.

Equation 19 and the experimental data in Table 1 can be used for validating the approximate expression in Eq. 17. As mentioned above, the relative error of this expression is $k_{AR}(1+r_{UD})/k_{ET} \quad k_{AR}/k_{IET}$, where the inequality follows from Eq. 19. For many full-length NOS enzymes in Table 1 (with the exception of bovine eNOS) k_{IET} is within the range of 35 – 45 s^{-1}. Using $k_{AR} \sim 10 \ s^{-1}$,[21–22] one can estimate the potential error of the approximate expression in Eq. 17 to be about 25% or smaller. Similar analysis can be performed for the bi-domain oxyFMN constructs, where the k_{IET} rate constants range between 262 s^{-1} (wt rat nNOS oxyFMN[21]) and 850 s^{-1} (wt murine iNOS oxyFMN[22]). The potential error of the approximate Eq. 17 in this case is smaller than 5%.

Some examples of using Eq. 10 for preliminary interpretation of experimental k_{IET} values summarized in Table 1 are discussed below.

i. The bulk IET rates can be used to estimate the minimal intrinsic k_{ET} rate constants using Eq. 19 and the experimental r_{UD} values. The inspection of Table 1 shows, however, that while there is a substantial number of k_{IET} entries, the r_{UD} values have only been measured for a limited number of samples. Moreover, even the available r_{UD} values most likely contain significant inaccuracies (partly

resulting from difficulties in the interpretation/assignment of the fluorescence components with different lifetimes), as can be deduced from the fact that some of them are mutually contradictory. For example, for nNOS oxyFMN without bound CaM, $[D]_o \sim 0$ was measured by pulsed EPR,[29] but at the same time, the $[D]_o$ values of $\sim 12\%$[33] and 19%[31] were estimated by FMN fluorescence lifetime measurements for the full-length nNOS without CaM (where the $[D]_o$ values should be smaller than for the oxyFMN construct). As another example, different r_{UD} values for the full-length rat nNOS with bound CaM resulted from two fluorescence lifetime measurements[31, 33] (see Table 1).

It is thus obvious that the conformational equilibrium measurements lag significantly behind the IET rate measurements both in number and, potentially, in accuracy, and at present can only be considered with great caution. For comparative considerations, we will therefore only use the r_{UD} values obtained by the same technique in the same set of measurements (there is currently only one example of such, given by the full-length murine iNOS and the corresponding oxyFMN construct[32]).

For the minimal k_{ET} estimates, we can use the overall minimal $r_{UD} = 2.6$ listed in Table 1. Although this value is for the oxyFMN construct, the minimal available r_{UD} for a full-length enzyme is not much greater ($r_{UD} = 2.9$ for the full-length rat nNOS[31]). Thus, from $k_{IET} = 850$ s^{-1} in murine iNOS oxyFMN, the minimal $k_{ET} = 3060$ s^{-1} can be estimated. Similarly, the minimal k_{ET} of about 940 s^{-1} can be estimated from $k_{IET} = 262$ s^{-1} for the oxyFMN construct of rat nNOS. If, however, $r_{UD} \approx 5.5$ determined for this enzyme by pulsed EPR[29] is used, then the minimal intrinsic ET rate becomes $k_{ET} \approx 1700$ s^{-1}, significantly closer to that estimated for iNOS oxyFMN.

For the full-length enzymes (excluding bovine eNOS), the bulk IET rates are within the range of $35 - 45$ s^{-1}, which results in minimal $k_{ET} \sim 135 - 175$ s^{-1} (for $r_{UD} = 2.9$[31]) or about twice greater using $r_{UD} = 4.7$.[33] These estimated minimal k_{ET} values are much smaller than those for the oxyFMN constructs, but it is not clear if such a cross-experiment comparison of minimal k_{ET} values would be meaningful at present, given the potential r_{UD} accuracy problems discussed above.

For the wt full-length bovine eNOS, the bulk IET rate is low (only 4.3 ± 1 s^{-1}). Based on the fluorescence lifetime data for the wt eNOS,[35] r_{UD} is estimated to be 4.0. The minimal k_{ET} value for the wt bovine eNOS is thus 22 ± 5 s^{-1}. For comparison, $r_{UD} = 8.6 \pm 2.9$ and 6 ± 2 can be obtained from the fluorescence decay and single-molecule fluorescence trajectory data for the S1179D mutant of bovine eNOS.[30] The larger r_{UD} found for the mutant eNOS contradicts the expectation that r_{UD} should be significantly smaller than in the wt because the phosphomimetic mutation doubles the synthase activity and has a stabilizing effect on the FMN-heme docking complex.[36-37] This again suggests that the available r_{UD} values are rather qualitative and might contain significant inaccuracies. Therefore, it is not clear if the slow bulk IET rate in eNOS is due to the decrease in k_{ET} or an increase in r_{UD} and k_{DU}, or both. Nonetheless, the minimal k_{ET} value for eNOS is obviously much smaller than those of nNOS and iNOS.

(ii) As mentioned above, the k_{IET} values for the full-length enzymes are significantly smaller than that observed for the oxyFMN construct: 35 s^{-1} *vs.* 850 s^{-1} in murine iNOS, 35 s^{-1} *vs.* 343 s^{-1} in human iNOS, and 43 s^{-1} *vs.* 262 s^{-1} in CaM-bound rat nNOS. Since in a full-length enzyme the FMN domain spends part of the time docked to the FNR domain (see Figure 1), the rate of formation of the FMN-heme docked state in a full-length protein is slower than in the corresponding oxyFMN construct. This results in decrease of k_{IET}, which is proportional to k_{UD}. The r_{UD} data for murine iNOS (full-length *vs.* oxyFMN) that were obtained in the same set of fluorescence lifetime experiments[32] support these considerations. In addition, it is plausible that either k_{DU} or k_{ET}, or both, are also affected by the presence or absence of the FNR domain in the studied protein. The complete understanding of the changes will only be possible when the direct experimental data on the conformational rate constants become available.

(iii) The IET rate in the oxyFMN construct of rat nNOS without CaM is an order of magnitude slower than in the enzyme with CaM (see Table 1). This can qualitatively be rationalized by considering the fact that the bound CaM facilitates the FMN-heme domain docking (through its own docking to the heme domain),[25] and without CaM either k_{UD} becomes very small or k_{DU} becomes very large, or both.

(iv) The experiments with human iNOS oxyFMN mutated at the FMN - heme domain linker (S562K, C563, and R536E mutations, see Table 1) have resulted in a decrease of k_{IET} for two of the mutants, S562K and R536E, with the effect for R536E being especially dramatic (~ 25-fold decrease of k_{IET}). The most likely reason for the observed IET rate changes is the decrease of k_{UD}. Such a strong effect of the R536E mutation is conceivable because the CaM-binding region of the FMN - heme domain linker together with CaM forms a hinge and pivots on the R536(NOS)/E47(CaM) pair.[38]

(v) The diffusion controlled k_{UD} depends on the solvent viscosity. Unless $k_{UD} \gg (k_{DU}, k_{ET})$, $k_{IET} \propto k_{UD}$, and it is expected that k_{IET} should become smaller as viscosity increases. Indeed, an approximately linear correlation between the viscosity and $1/k_{IET}$ was observed.[16]

(vi) The E546N mutation of human iNOS oxyFMN has resulted in a 2.5-fold decrease of k_{IET}, and a comparable (~ two-fold) increase in r_{UD} was observed.[14] The conserved E546 residue is located on the FMN domain surface and is involved in the FMN - heme domain docking interface. The observed decrease in k_{IET} in this case is most likely related to the increase in k_{DU}.

Conclusions

In this work, we have provided an analytical solution of kinetic equations describing the NOS LFP experiments. The exact and approximate formulae expressing the observed bulk IET and CO rebinding rates through the intrinsic rate constants will be useful for interpreting the LFP data from various native and modified NOS enzymes. The analysis of

these expressions has revealed that in order to fully interpret the LFP results in terms of the intrinsic ET rates, direct experimental data on the docking equilibrium and conformational change rate constants are necessary. The equilibrium data can be obtained by pulsed EPR[29] and/or fluorescence lifetime[31] measurements, while the absolute conformational rate constants may be measurable using single-molecule fluorescence resonance energy transfer.[30, 39–40] A combined approach consisting of all these measurements and numerical simulations of the IET kinetics using either a numerical solution of the kinetic equations or their exact solution without the CO rebinding obtained in this work will allow one to achieve a detailed understanding of the role of various structural and dynamic factors in determining the NOS IET and NO production efficiency. In particular, it would be interesting to conduct this kind of studies in parallel for the three NOS isoforms and correlate the intrinsic rate constants with the FMN···heme distances in the FMN/heme docking complexes.[41] Such a work will significantly advance our understanding of the structural determinants underlying the significantly different IET rates.

The mathematical expressions derived in this work will also be applicable, with minor modifications, for interpreting the IET kinetics in other modular enzymes whose function depends on conformational mobility, *e.g.*, sulfite oxidase[42] or the Rieske protein of the cytochrome *bc*1 complex.[22] This work should inspire further systematic measurements of the conformational change rates and conformational equilibria, and investigations of their effect on the electron transfer efficiency in modular enzymes.

Acknowledgments

Abbreviations

NO	nitric oxide
NOS	nitric oxide synthase
eNOS	endothelial NOS
iNOS	inducible NOS
nNOS	neuronal NOS
CaM	calmodulin
FAD	flavin adenine dinucleotide
FMN	flavin mononucleotide
FNR	ferredoxin-NADP reductase
ET	electron transfer
IET	interdomain electron transfer

EPR	electron paramagnetic resonance
LFP	laser flash photolysis
oxyFMN	bi-domain NOS construct in which only oxygenase and FMN domains along with CaM-binding region are present

References

1. Alderton WK, Cooper CE, Knowles RG. Nitric Oxide Synthases: Structure, Function and Inhibition. Biochem. J. 2001; 357:593–615. [PubMed: 11463332]

2. Poulos TL. Heme Enzyme Structure and Function. Chem. Rev. 2014; 114:3919–3962. [PubMed: 24400737]

3. Panda K, Ghosh S, Stuehr DJ. Calmodulin Activates Intersubunit Electron Transfer in the Neuronal Nitric-Oxide Synthase Dimer. J. Biol. Chem. 2001; 276:23349–23356. [PubMed: 11325964]

4. Roman LJ, Martasek P, Masters BSS. Intrinsic and Extrinsic Modulation of Nitric Oxide Synthase Activity. Chem. Rev. 2002; 102:1179–1189. [PubMed: 11942792]

5. Stuehr DJ, Santolini J, Wang ZQ, Wei CC, Adak S. Update on Mechanism and Catalytic Regulation in the No Synthases. J. Biol. Chem. 2004; 279:36167–36170. [PubMed: 15133020]

6. Feng C. Mechanism of Nitric Oxide Synthase Regulation: Electron Transfer and Interdomain Interactions. Coord. Chem. Rev. 2012; 256:393–411. [PubMed: 22523434]

7. Noble MA, Munro AW, Rivers SL, Robledo L, Daff SN, Yellowlees LJ, Shimizu T, Sagami I, Guillemette JG, Chapman SK. Potentiometric Analysis of the Flavin Cofactors of Neuronal Nitric Oxide Synthase. Biochemistry. 1999; 38:16413–16418. [PubMed: 10600101]

8. Gao YT, Smith SME, Weinberg JB, Montgomery HJ, Newman E, Guillemette JG, Ghosh DK, Roman LJ, Martasek P, Salerno JC. Thermodynamics of Oxidation-Reduction Reactions in Mammalian Nitric-Oxide Synthase Isoforms. J. Biol. Chem. 2004; 279:18759–18766. [PubMed: 14715665]

9. Daff S, Noble MA, Craig DH, Rivers SL, Chapman SK, Munro AW, Fujiwara S, Rozhkova E, Sagami I, Shimizu T. Control of Electron Transfer in Neuronal No Synthase. Biochem. Soc. Trans. 2001; 29:147–152. [PubMed: 11356143]

10. Panda K, Adak S, Konas D, Sharma M, Stuehr DJ. A Conserved Aspartate (Asp-1393) Regulates Nadph Reduction of Neuronal Nitric-Oxide Synthase - Implications for Catalysis. J. Biol. Chem. 2004; 279:18323–18333. [PubMed: 14966111]

11. Sheng Y, Zhong L, Guo D, Lau G, Feng C. Insight into Structural Rearrangements and Interdomain Interactions Related to Electron Transfer between Flavin Mononucleotide and Heme in Nitric Oxide Synthase: A Molecular Dynamics Study. J. Inorg. Biochem. 2015 in press.

12. Hollingsworth SA, Holden JK, Li H, Poulos TL. Elucidating Nitric Oxide Synthase Domain Interactions by Molecular Dynamics. Protein Sci. 2015 in press.

13. Leferink NGH, Hay S, Rigby SEJ, Scrutton NS. Towards the Free Energy Landscape for Catalysis in Mammalian Nitric Oxide Synthases. FEBS J. 2015; 282:3016–3029. [PubMed: 25491181]

14. Li W, Chen L, Lu C, Elmore BO, Astashkin AV, Rousseau DL, Yeh S-R, Feng C. Regulatory Role of Glu546 in Flavin Mononucleotide — Heme Electron Transfer in Human Inducible Nitric Oxide Synthase. Inorg. Chem. 2013; 52:4795–4801. [PubMed: 23570607]

15. Li W, Fan W, Chen L, Elmore B, Piazza M, Guillemette J, Feng C. Role of an Isoform-Specific Serine Residue in Fmn–Heme Electron Transfer in Inducible Nitric Oxide Synthase. J. Biol. Inorg. Chem. 2012; 17:675–685. [PubMed: 22407542]

16. Li W, Fan W, Elmore BO, Feng C. Effect of Solution Viscosity on Intraprotein Electron Transfer between the Fmn and Heme Domains in Inducible Nitric Oxide Synthase. FEBS Lett. 2011; 585:2622–2626. [PubMed: 21803041]

17. Feng C, Taiakina V, Ghosh DK, Guillemette JG, Tollin G. Intraprotein Electron Transfer between the Fmn and Heme Domains in Endothelial Nitric Oxide Synthase Holoenzyme. Biochimica et Biophysica Acta (BBA) - Proteins & Proteomics. 2011; 1814:1997–2002. [PubMed: 21864726]

18. Feng C, Fan W, Dupont A, Guy Guillemette J, Ghosh DK, Tollin G. Electron Transfer in a Human Inducible Nitric Oxide Synthase Oxygenase/Fmn Construct Co-Expressed with the N-Terminal Globular Domain of Calmodulin. FEBS Lett. 2010; 584:4335–4338. [PubMed: 20868689]

19. Feng CJ, Dupont A, Nahm N, Spratt D, Hazzard JT, Weinberg J, Guillemette J, Tollin G, Ghosh DK. Intraprotein Electron Transfer in Inducible Nitric Oxide Synthase Holoenzyme. J. Biol. Inorg. Chem. 2009; 14:133–142. [PubMed: 18830722]

20. Feng CJ, Roman LJ, Hazzard JT, Ghosh DK, Tollin G, Masters BSS. Deletion of the Autoregulatory Insert Modulates Intraprotein Electron Transfer in Rat Neuronal Nitric Oxide Synthase. FEBS Lett. 2008; 582:2768–2772. [PubMed: 18625229]

21. Feng CJ, Tollin G, Holliday MA, Thomas C, Salerno JC, Enemark JH, Ghosh DK. Intraprotein Electron Transfer in a Two-Domain Construct of Neuronal Nitric Oxide Synthase: The Output State in Nitric Oxide Formation. Biochemistry. 2006; 45:6354–6362. [PubMed: 16700546]

22. Feng CJ, Thomas C, Holliday MA, Tollin G, Salerno JC, Ghosh DK, Enemark JH. Direct Measurement by Laser Flash Photolysis of Intramolecular Electron Transfer in a Two-Domain Construct of Murine Inducible Nitric Oxide Synthase. J. Am. Chem. Soc. 2006; 128:3808–3811. [PubMed: 16536556]

23. Kawatsu T, Beratan DN. Electron Transfer between Cofactors in Protein Domains Linked by a Flexible Tether. Chem. Phys. 2006; 326:259–269.

24. Feng C, Chen L, Li W, Elmore BO, Fan W, Sun X. Dissecting Regulation Mechanism of the Fmn to Heme Interdomain Electron Transfer in Nitric Oxide Synthases. J. Inorg. Biochem. 2014; 130:130–140. [PubMed: 24084585]

25. Smith BC, Underbakke ES, Kulp DW, Schief WR, Marletta MA. Nitric Oxide Synthase Domain Interfaces Regulate Electron Transfer and Calmodulin Activation. Proc Natl Acad Sci U S A. 2013; 110:E3577–E3586. [PubMed: 24003111]

26. Moser CC, Keske JM, Warncke K, Farid RS, Dutton PL. Nature of Biological Electron Transfer. Nature. 1992; 355:796–802. [PubMed: 1311417]

27. Page CC, Moser CC, Chen XX, Dutton PL. Natural Engineering Principles of Electron Tunnelling in Biological Oxidation-Reduction. Nature. 1999; 402:47–52. [PubMed: 10573417]

28. Feng CJ, Tollin G, Hazzard JT, Nahm NJ, Guillemette JG, Salerno JC, Ghosh DK. Direct Measurement by Laser Flash Photolysis of Intraprotein Electron Transfer in a Rat Neuronal Nitric Oxide Synthase. J. Am. Chem. Soc. 2007; 129:5621–5629. [PubMed: 17425311]

29. Astashkin AV, Chen L, Zhou X, Li H, Poulos TL, Liu KJ, Guillemette JG, Feng C. Pulsed Electron Paramagnetic Resonance Study of Domain Docking in Neuronal Nitric Oxide Synthase: The Calmodulin and Output State Perspective. J. Phys. Chem. A. 2014; 118:6864–6872. [PubMed: 25046446]

30. Arnett DC, Persechini A, Tran Q-K, Black DJ, Johnson CK. Fluorescence Quenching Studies of Structure and Dynamics in Calmodulin–Enos Complexes. FEBS Lett. 2015; 589:1173–1178. [PubMed: 25871521]

31. Salerno JC, Ray K, Poulos T, Li H, Ghosh DK. Calmodulin Activates Neuronal Nitric Oxide Synthase by Enabling Transitions between Conformational States. FEBS Lett. 2013; 587:44–47. [PubMed: 23159936]

32. Ghosh DK, Ray K, Rogers AJ, Nahm NJ, Salerno JC. Fmn Fluorescence in Inducible Nos Constructs Reveals a Series of Conformational States Involved in the Reductase Catalytic Cycle. FEBS J. 2012; 279:1306–1317. [PubMed: 22325715]

33. Brunner K, Tortschanoff A, Hemmens B, Andrew PJ, Mayer B, Kungl AJ. Sensitivity of Flavin Fluorescence Dynamics in Neuronal Nitric Oxide Synthase to Cofactor-Induced Conformational Changes and Dimerization. Biochemistry. 1998; 37:17545–17553. [PubMed: 9860870]

34. Ghosh DK, Holliday MA, Thomas C, Weinberg JB, Smith SME, Salerno JC. Nitric-Oxide Synthase Output State - Design and Properties of Nitric-Oxide Synthase Oxygenase/Fmn Domain Constructs. J. Biol. Chem. 2006; 281:14173–14183. [PubMed: 16461329]

35. Salerno JC, Ghosh DK, Razdan R, Helms KA, Brown CC, McMurry JL, Rye EA, Chrestensen CA. Endothelial Nitric Oxide Synthase Is Regulated by Erk Phosphorylation at Ser602. Biosci Rep. 2014; 34

36. Persechini A, Tran QK, Black DJ, Gogol EP. Calmodulin-Induced Structural Changes in Endothelial Nitric Oxide Synthase. FEBS Lett. 2013; 587:297–301. [PubMed: 23266515]

37. Tran QK, Leonard J, Black DJ, Nadeau OW, Boulatnikov IG, Persechini A. Effects of Combined Phosphorylation at Ser-617 and Ser-1179 in Endothelial Nitric-Oxide Synthase on Ec50(Ca2+) Values for Calmodulin Binding and Enzyme Activation. J. Biol. Chem. 2009; 284:11892–11899. [PubMed: 19251696]

38. Xia C, Misra I, Iyanagi T, Kim J-JP. Regulation of Interdomain Interactions by Calmodulin in Inducible Nitric Oxide Synthase. J. Biol. Chem. 2009; 284:30708–30717. [PubMed: 19737939]

39. He Y, Haque MM, Stuehr DJ, Lu HP. Single-Molecule Spectroscopy Reveals How Calmodulin Activates No Synthase by Controlling Its Conformational Fluctuation Dynamics. Proc Natl Acad Sci U S A. 2015; 112:11835–11840. [PubMed: 26311846]

40. Weiss S. Fluorescence Spectroscopy of Single Biomolecules. Science. 1999; 283:1676–1683. [PubMed: 10073925]

41. Astashkin AV, Elmore BO, Fan W, Guillemette JG, Feng C. Pulsed Epr Determination of the Distance between Heme Iron and Fmn Centers in a Human Inducible Nitric Oxide Synthase. J. Am. Chem. Soc. 2010; 132:12059–12067. [PubMed: 20695464]

42. Feng C, Tollin G, Enemark JH. Sulfite Oxidizing Enzymes. Biochim. Biophys. Acta. 2007; 1774:527–39. [PubMed: 17459792]
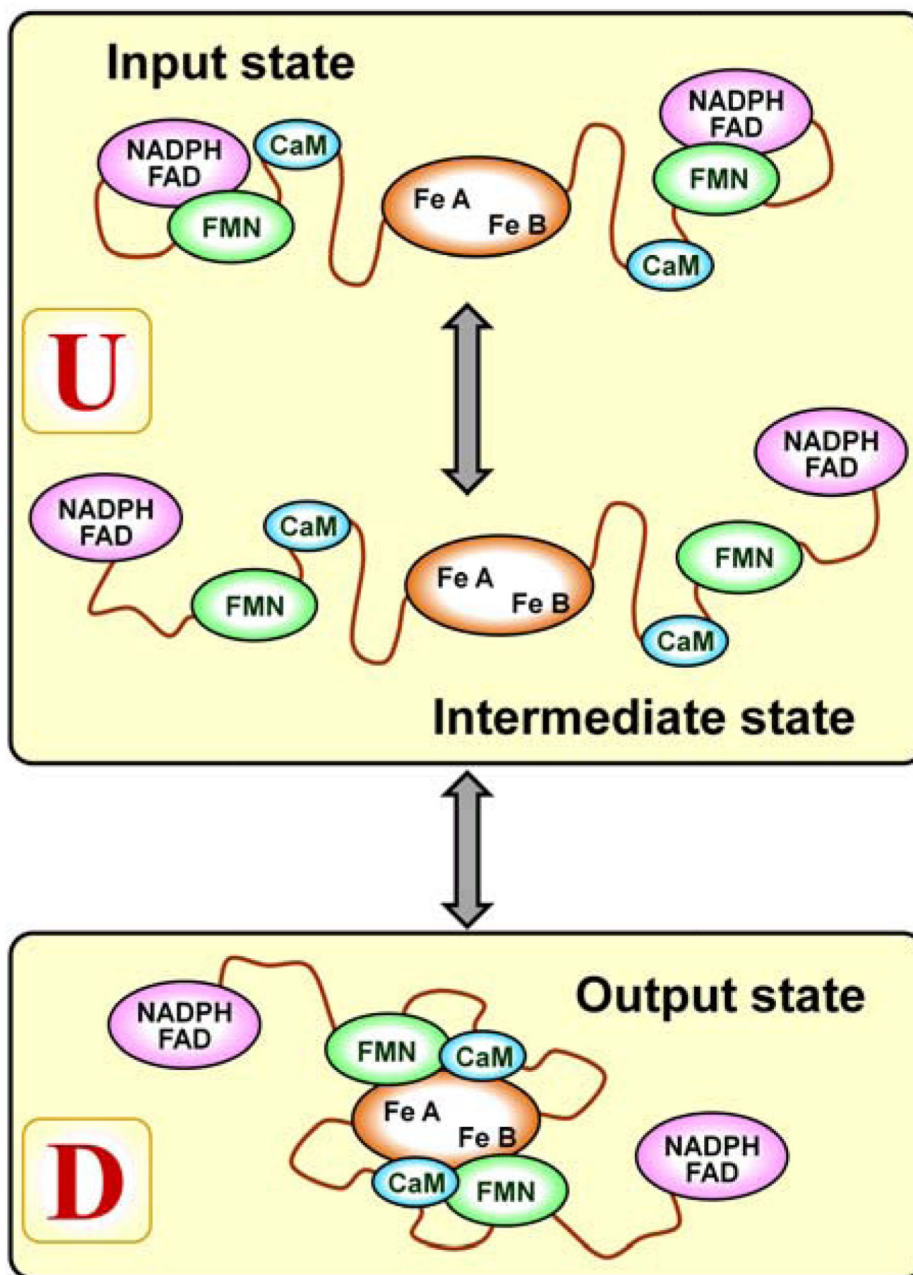
Conformational states of CaM-bound NOS

Figure 1.
Conformational states of CaM-bound NOS. In the input state, the FMN domain is docked to the FAD- and NADPH-binding FNR domain, where it receives an electron to be transported to the heme domain. In the intermediate state, the FMN domain is not docked to other domains and is either transporting an electron toward the heme domain or returns to the FNR domain for a new electron. In the output state, the FMN domain is docked to the heme domain. In this state, the FMN-heme IET event takes place. In this work, the input and

intermediate states are combined into the undocked (with respect to the FMN-heme docking) state, U, while the output state is referred to as the docked state, D.
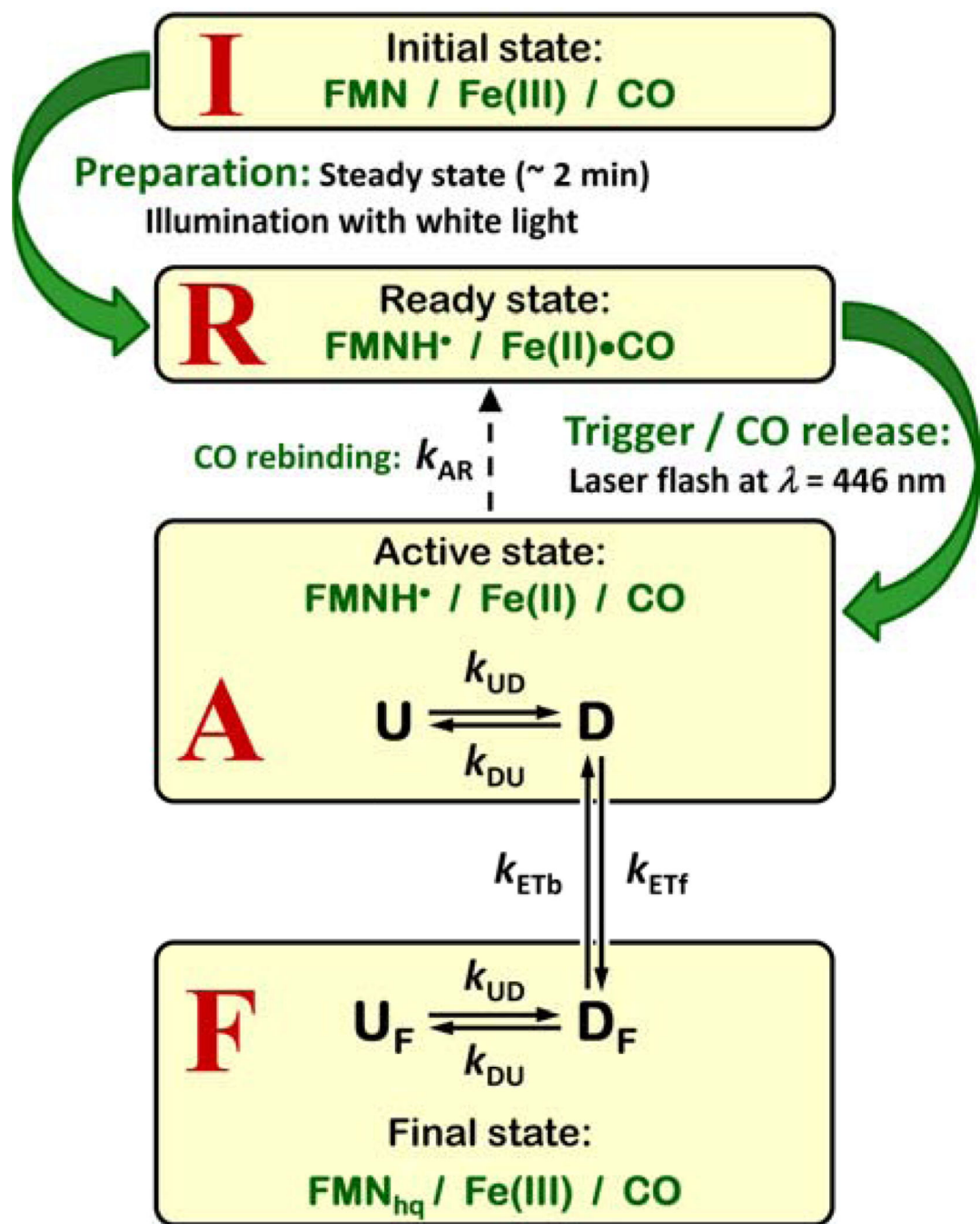
Figure 2.
NOS redox states and relevant IET and conformational change kinetics in the context of the LFP experiment.
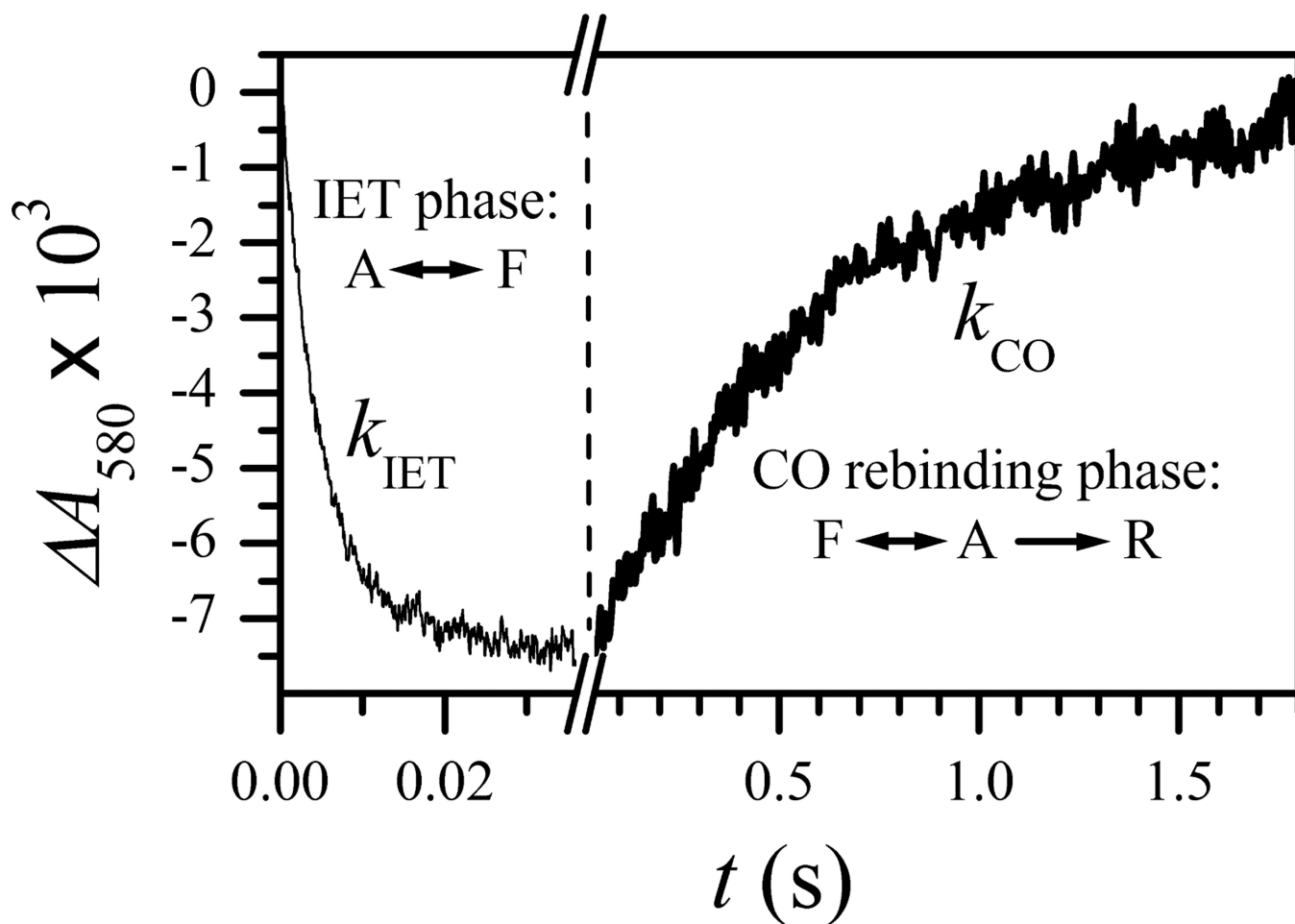
Figure 3.
The LFP trace obtained for the S562 mutant of human iNOS oxyFMN. This trace is shown
as an example to explain the typical features of the kinetic data obtained in an LFP
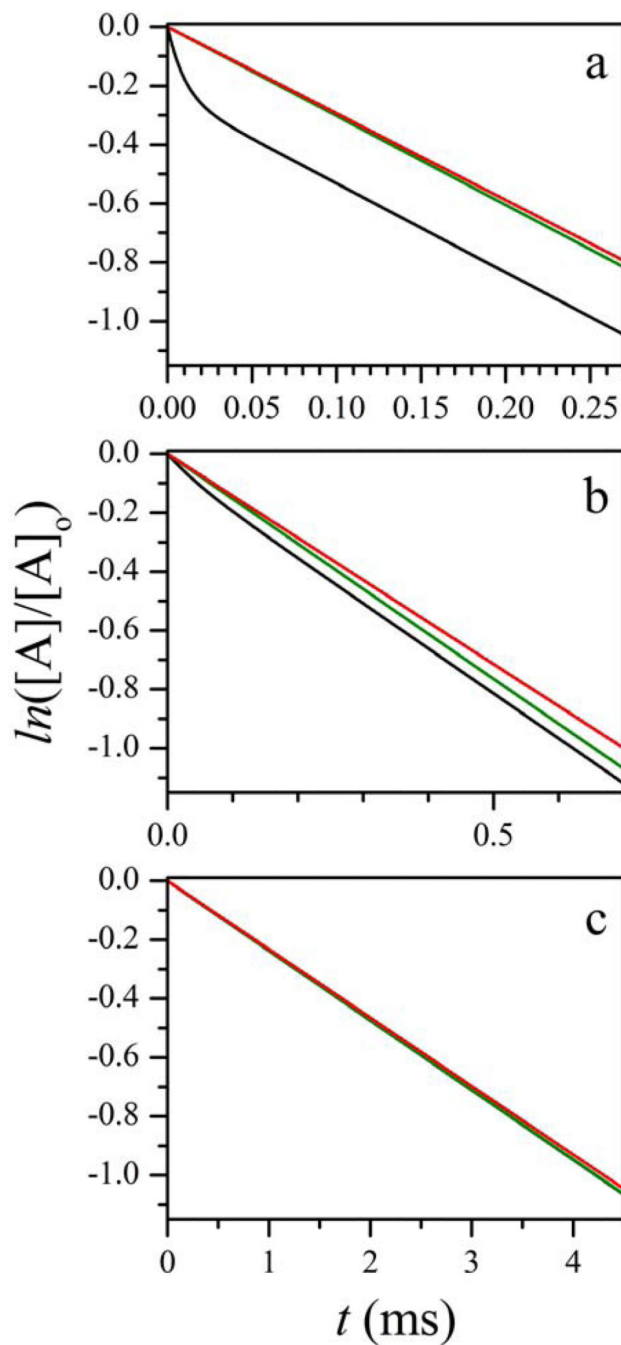experiment. The experimental details are described in the original work.[15]

Figure 4.
Calculated kinetics of the active state population in an LFP experiment for $k_{AR} = 0$ (no CO rebinding). Calculation parameters: $k_{DU} = 10$ ms^{-1}; $k_{UD} = 3.33$ ms^{-1}; $k_{ETf} = 100$, 10, and 1 ms^{-1} in panels a, b, and c, respectively; $k_{ETb} = 0$. Black trace in each panel is calculated using the exact expressions given by Eqs. 5 and 6. Green trace is a monoexponential kinetic given by Eq. 9, calculated using the exact expression for k_{IET} in Eq. 10. Red trace is a monoexponential kinetic given by Eq. 9, calculated using the approximate expression for k_{IET} in Eq. 10.
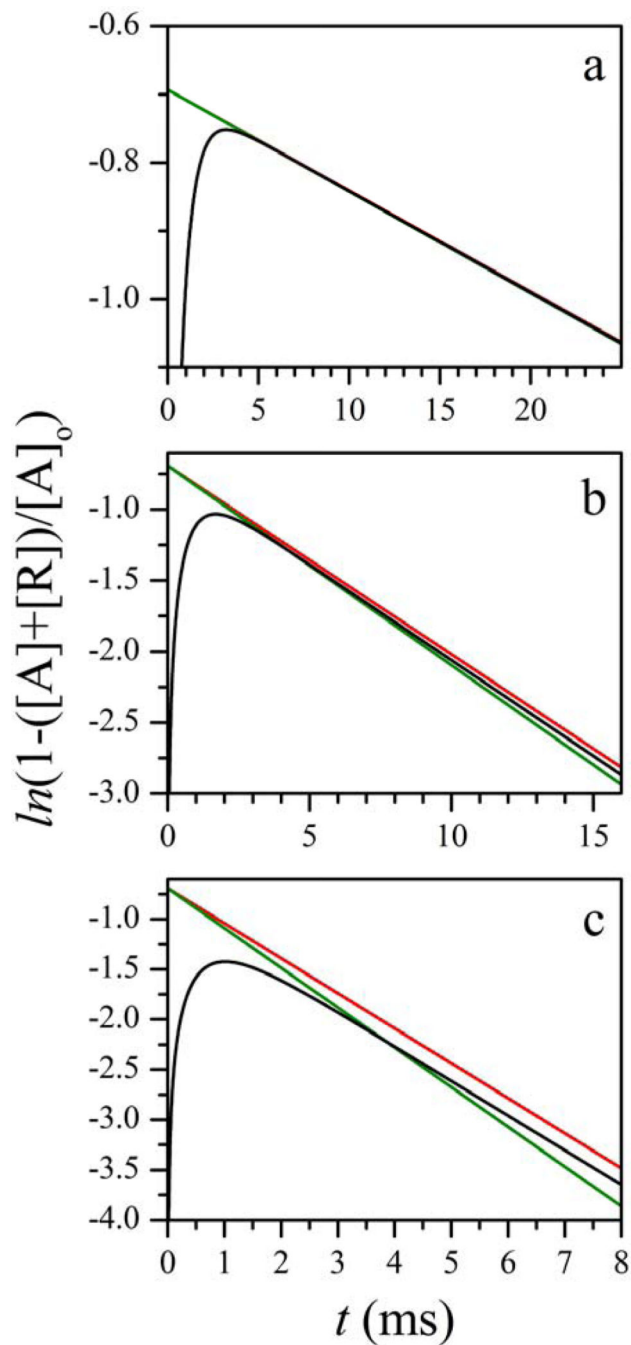
Figure 5.
Calculated kinetics of the total population of the active and ready states in an LFP experiment for $k_{AR} > 0$ (with CO rebinding). Calculation parameters: $k_{DU} = 10$ ms^{-1}; $k_{UD} = 3$ ms^{-1}; $k_{ETf} = k_{ETb} = 5$ ms^{-1}; $k_{AR} = 0.03$, 0.3, and 1 ms^{-1} in panels a, b, and c, respectively. Black trace in each panel represents a numerical solution of Eqs. 3 for [A] + [R]. Green trace is a monoexponential kinetics for [A] + [R] given by Eqs. 15, calculated using the exact (for the equilibrium model) expression for k_{CO} in Eq. 16. Red trace is a monoexponential

kinetics for [A] + [R] given by Eqs. 15, calculated using the approximate expression for k_{CO} in Eq. 16.

Table 1

The bulk IET rate constants and the ratios of undocked/docked state populations (r_{UD}) in NOS proteins. The IET rate constants shown are the averages over the ranges given in the references.

NOS protein	k_{IET} (s^{-1})	Ref.	r_{UD}	Ref.
wt murine iNOS oxyFMN	850	[22]	2.6	[32]
wt full-length murine iNOS	35	[19]	$\gg 1$ [a]	[32]
wt human iNOS oxyFMN	343	[16, 19]	_[b]	
wt full-length human iNOS	35	[19]	-	
E546N human iNOS oxyFMN	139	[14]	-	
S562K human iNOS oxyFMN	192	[15]	-	
C563R human iNOS oxyFMN	340	[15]	-	
R536E human iNOS oxyFMN	13.6	[15]	-	
Human iNOS oxyFMN + NCaM	93	[18]	-	
wt rat nNOS oxyFMN; no CaM	22	[21]	$\gg 1$ [a]	[29]
wt rat nNOS oxyFMN with bound CaM	262	[21]	5.5	[29]
wt full-length rat nNOS	43	[20, 28]	2.9	[31]
AR-deletion mutant of full-length rat nNOS	44	[20]	4.7	[33]
wt full-length bovine eNOS	4.3	[17]	-	

[a]"$\gg 1$" indicates that no equilibrium docked state population was reliably detected ([D]$_O \sim 0$).

[b]"-" indicates that the value is not determined/reported.